Topological properties of individual gray matter morphological networks in identifying the preclinical stages of Alzheimer's disease: a preliminary study

Hongyuan Ding[1]#, Zhihao Wang[2]#, Yin Tang[3], Tong Wang[4], Ming Qi[1], Weiqiang Dou[5], Long Qian[5], Yaxin Gao[6,7], Qian Zhong[8], Xi Yang[9], Huifang Tian[9], Ling Zhang[1], Yi Zhu[4]

[1]Department of Radiology, The First Affiliated Hospital of Nanjing Medical University, Nanjing, China; [2]School of Biological Science & Medical Engineering, Southeast University, Nanjing, China; [3]Department of Medical Imaging, Jingjiang People's Hospital, Jingjiang, China; [4]Rehabilitation Medicine Center, The First Affiliated Hospital of Nanjing Medical University, Nanjing, China; [5]MR Research, GE Healthcare, Beijing, China; [6]Department of Rehabilitation, The Affiliated Suzhou Hospital of Nanjing Medical University, Suzhou, China; [7]Gusu School, Nanjing Medical University, Suzhou, China; [8]Department of Rehabilitation, Nanjing Drum Tower Hospital Clinical College of Nanjing Medical University, Nanjing, China; [9]School of Rehabilitation Medicine, Nanjing Medical University, Nanjing, China

Contributions: (I) Conception and design: Y Zhu, L Zhang, T Wang, M Qi; (II) Administrative support: Y Zhu, M Qi; (III) Provision of study materials or patients: Q Zhong, X Yang, H Tian; (IV) Collection and assembly of data: H Ding, Y Tang, Y Gao; (V) Data analysis and interpretation: Z Wang, W Dou, L Qian; (VI) Manuscript writing: All authors; (VII) Final approval of manuscript: All authors.

#These authors contributed equally to this work and should be considered as co-first authors.

Correspondence to: Yi Zhu, PhD, MD. Rehabilitation Medicine Center, The First Affiliated Hospital of Nanjing Medical University, 300 Guangzhou Road, Gulou District, Nanjing 210029, China. Email: lucky.zyx@163.com; Ling Zhang, MSc. Department of Radiology, The First Affiliated Hospital of Nanjing Medical University, 300 Guangzhou Road, Gulou District, Nanjing 210029, China. Email: zl_phx@126.com.

Background: Subjective cognitive decline (SCD) and mild cognitive impairment (MCI) are preclinical stages of Alzheimer's disease (AD). Individual biomarkers are essential for evaluating altered neurological outcomes at both SCD and MCI stages for early diagnosis and intervention of AD. In this study, we aimed to investigate the relationships between topological properties of the individual brain morphological network and clinical cognitive performances among healthy controls (HCs) and patients with SCD or MCI.

Methods: The topological measurements of individual morphological networks were analyzed using graph theory, and inter-group differences of standard graph topology were correlated and regressed to scores of clinical cognitive functions.

Results: Compared with HCs, the topology of the individual morphological networks in SCD and MCI patients was significantly altered. At the global level, altered topology was characterized by lower global efficiency, shorter characteristics path length, and normalized characteristics path length [all P<0.05, false discovery rate (FDR) corrected]. In addition, at the regional level, SCD and MCI patients exhibited abnormal degree centrality in the caudate nucleus and nodal efficiency in the caudate nucleus, right insula, lenticular nucleus, and putamen (all P<0.05, FDR corrected).

Conclusions: The topological features of individual gray matter morphological networks may serve as biomarkers to improve disease prognosis and intervention in the early stages of AD, namely SCD and MCI. Moreover, these findings may further elucidate the relationships between brain morphological alterations and cognitive dysfunctions in SCD and MCI.

Keywords: Subjective cognitive decline (SCD); mild cognitive impairment (MCI); normalized individual gray matter morphological network; graph theory analysis; cognitive performance; early detection

Introduction

Alzheimer's disease (AD), resulting in approximately 50–80% of all dementia cases (1), is a progressive and irreversible neurodegenerative disorder. Currently, no disease modifying therapy is available for AD and applied clinical drug trials feature a high risk of failure (2). The clinical hypothesis for such outcomes is that AD patients have a long preclinical phase (2) and their brain pathology emerges years before the manifestation of clinical cognitive impairment (3). Recently, studies have investigated the earlier clinical stages of neurodegeneration that bear a high risk of progression to AD, including subjective cognitive decline (SCD), the preclinical stage of AD, and mild cognitive impairment (MCI), the early symptomatic stage of AD.

SCD is characterized by self-perceived deterioration of cognitive performance, but does not usually represent clinical neuropsychological dysfunction (4). Most studies have reported that SCD is the earliest alert of AD, and that individuals with SCD are at higher risk of developing MCI or even AD (5-7). In comparison, MCI refers to objective cognitive impairment but with general preservation of daily cognitive functioning compared to dementia (8,9), and is regarded as a transitional phase between the cognitive changes associated with aging and early AD (10,11). Thus, it is crucial to find effective biomarkers to identify SCD and MCI, so as to diagnose and intervene in AD at earlier stages (6,12).

Amyloid accumulation in the brain is one of the initially altered biomarkers that may be associated with the occurrence of AD (13-15). However, the abnormality of amyloid level is only weakly associated with the rate of clinical cognitive decline, probably because it plateaus at a very early stage of the disease (16). Alternatively, the loss of synapses has been robustly related to dementia (17). Synaptic dysfunction disrupts brain connectivity, and increasing evidence shows that brain connectivity and networks start changing early during the progression of AD (18-20). Therefore, topological properties of brain networks may be sensitive to incipient brain damage (21).

Magnetic resonance imaging (MRI), due to its intrinsic properties of high image resolution and well depicted tissue contrast, may show promise in identifying imaging markers. Meanwhile, graph theory analysis has been a useful tool to assess brain function with topological measurements. With this method, different modalities of MRI data, including structural MRI, diffusion MRI, and functional MRI (fMRI), have been used to construct brain networks and study altered brain connectivity in a variety of neurodegenerative diseases (22-25). However, relative to structural MRI, diffusion and fMRI usually require longer acquisition time and are thus more challenging due to motion artifacts for patients with neurological and psychiatric diseases. Therefore, high resolution structural MRI has attracted considerable interest for analyzing brain morphological networks in recent years (18,20,26-28). Moreover, an inter-individual level analysis was proposed recently, based on cortical similarities in gray matter morphology within single cases (19,21,29-34). In this method, brain network graphs were constructed with nodes representing cortical regions and edges characterizing connected cortical regions, which share significant statistical similarities. Compared to the often-used volumetric features (9%) in the construction of morphological networks, increased variance in measurements of general cognitive decline can be largely explained by using the topological properties of the morphological network (32%) (29).

Some studies have applied this recently proposed method to study single subject gray matter morphological network alterations in SCD, MCI, or AD (21,29,30,32). For AD patients, the topology randomness of the brain morphological network has a positive correlation with the levels of cognitive impairment (29,30,32). Moreover, at predementia stages, such as SCD or MCI, the alterations of topological properties of the gray matter network can predict faster atrophy in brain regions related to AD progression (35), and identify patients featuring fast clinical progression (21,36). These studies demonstrated a certain potential of topological measures of individual morphological networks over other reported biomarkers in predicting clinical cognitive decline. Based on these promising findings, we assumed that this method may have potential for distinguishing the two preclinical phases of AD in the aspect of gray matter morphological network alterations, by comparing with healthy controls (HCs),

and for further predicting the clinical cognitive differences based on the topological property alterations. To the best our knowledge, this concept had not been previously investigated.

Therefore, the aim of this study was first to explore the differences of individual morphological network features among HCs, SCD, and MCI, and second to identify potential imaging biomarkers for early diagnosis and intervention of SCD and MCI.

Methods

Participants

A total of 78 non-demented patients (SCD =39, MCI =39) were included in this study. Additionally, 26 (13 males and 13 females) HCs matched with both SCD and MCI groups for sex, years of education, hypertension, diabetes, lacunar infraction, and Hachinski Ischemic Scale (HIS), were also recruited. This study was conducted in accordance with the Declaration of Helsinki (as revised in 2013). The study was approved by the Ethics Committee of the First Affiliated Hospital of Nanjing Medical University, and written informed consent was provided by each of the participants.

Patients with MCI all met the following criteria: (I) age between 55 and 85 years; (II) diagnosis of MCI according to the latest standards of the National Institute on Aging and Alzheimer's Association guidelines (9); (III) the presence of memory complaint for more than 6 months but preserved activities of daily living.

The criteria of SCD were defined as follows: (I) age between 55 and 85 years; (II) the results of neuropsychological examination test were normal, or although there was some cognitive impairment, it did not meet the neuropsychological diagnostic standard of MCI; (III) according to the chief complaint, there was cognitive impairment compared with the healthy state, and there were no related acute events.

The criteria of the HC group were as follows: (I) no chief complaints of cognitive impairment; (II) cognitive test failed to meet the standard of SCD and MCI.

The exclusion criteria were as follows: (I) diagnosis of vascular dementia; (II) the score of the HIS was >4; (III) failure to cooperate with the cognitive function examination; (IV) complication with severe illness such as diabetes or cardiovascular disease, cerebrovascular disease, liver disease, and mental illness; (V) structural abnormalities such as brain tumor, subdural hematoma, head trauma, or a neurological or psychiatric disorder that could impact cognitive functions; (VI) lack of complete demographic information and poor magnetic resonance (MR) image quality.

Clinical performance evaluation

Each participant was assessed with multiple clinical scales, including the following: (I) general cognitive function assessed by Mini-Mental State Examination (MMSE), which is the most commonly used screening scale for dementia. A higher MMSE score indicates better cognitive function (37); (II) short-term memory assessed by Auditory-Verbal Learning Test (AVLT) (38), using delayed recall and recognition; (III) executive function assessed by the Trail Making Test (TMT) A&B (39); (IV) language function assessed by Animal Verbal Fluency Test (AVFT) (40) and Boston Naming Test (BNT) (41).

MRI data acquisition

All MRI experiments were performed on a 3-T MRI system (Discovery 750 W, GE Healthcare, Chicago, IL, USA) with a 24-channel phased array head coil employed. We acquired 3-dimensional (3D) 1-mm isotropic high-resolution T1-weighted (T1w) brain images using a spoiled gradient echo-based 3D-brain volume imaging (BRAVO) sequence for each case, with the scan parameters shown as follows: repetition time (TR) =8.5 ms, echo time (TE) =3.2 ms, flip angle =12°, matrix size =256×256, field of view (FOV) =256×256 mm^2, slice thickness =1 mm, number of slices =188, and bandwidth =31.25 kHz. The scan time was less than 5 minutes.

MRI data analysis

High-resolution T1w structural data were preprocessed with Computational Anatomy Toolbox (http://www.neuro.uni-jena.de/cat/) and SPM12 (https://www.fil.ion.ucl.ac.uk/spm/software/spm12/) in MATLAB (R2021b, MathWorks, Natick, MA, USA). Briefly, individual T1w images were segmented into grey matter, white matter, and cerebrospinal fluid via the standard segmentation model. All automatic segmentation results were first visually confirmed and then spatially normalized to the Montreal Neurological Institute (MNI) space, with the classic AAL90 template. Finally, the data were downsampled to 2×2×2 mm^3 and spatially smoothed with Gaussian kernel with a full width at half maximum of 6 mm.

In the normalized individual morphological network, nodes were defined as the anatomical regions in the automated anatomical labeling (AAL) atlas, and edges were defined as the interregional similarity measured with the multivariate Euclidean distances (MEDs) approach. The edge of $e(X,Y)$ between each pair of nodes (X,Y) in the morphological network was computed as follows (42):

$$e(X,Y) = \frac{n_1 n_2}{n_1 + n_2}\left(\frac{2}{n_1 n_2}\sum_{i=1}^{n_1}\sum_{j=1}^{n_2}\left\|x_i - y_j\right\|_2 - \frac{1}{n_1^2}\sum_{i=1}^{n_1}\sum_{j=1}^{n_1}\left\|x_i - x_j\right\|_2 - \frac{1}{n_2^2}\sum_{i=1}^{n_2}\sum_{j=1}^{n_2}\left\|y_i - y_j\right\|_2\right) \quad [1]$$

where $X = \{x_1, \ldots, x_n\}$ and $Y = \{y_1, \ldots, y_n\}$, x_i, and y_i denote imaging intensity of each voxel in region X and Y, respectively. In addition, n_1 and n_2 are the number of voxels in X and Y. The edge of $e(X,Y)$ influences the morphological feature distribution; when inter-regions have the same morphological feature, $e(X,Y) = 0$. Further, a normalization of min–max between regions of X and Y was performed to minimize possible bias in different regions across different participants. The similarity-based connectivity value was converted with the following equation:

$$c(X,Y) = \exp\left(-\frac{e(X,Y) - e_{\min}}{e_{\max} - e_{\min}}\right) \quad [2]$$

Finally, a 90×90 similarity-based connectivity matrix for each participant was obtained; the value range was circumscribed from 0 to 1, of which 1 represents identical morphological feature distributions between the 2 regions.

Topological properties of the individual morphological network were calculated with the GRETNA software (43). A set of sparsity (S) thresholds (0.10< S <0.40, with a step of 0.01) were applied to the morphological network correlation matrices to ensure their small-worldness. This step transformed the weighted network into binary graphs. By varying the sparsity thresholds from 0.1 to 0.4 with an increment of 0.01, we obtained different morphological network structures and different values of the topological metrics accordingly. To summarize the overall topological features of the morphological networks across different sparsity thresholds, we computed both global and regional network metrics at each sparsity threshold, and then integrated them via the area under the curve (AUC). The AUC of a topological metric was calculated by plotting the values against the corresponding sparsity thresholds and estimated using the trapezoidal rule. This resulted in a single value that reflects the average topological property of the network over a range of sparsity levels.

The global topological measurements were performed in terms of network efficiency and small-world parameters. For network efficiency, the further divided global efficiency (Eg) and local efficiency (Eloc) were assessed; for small-world parameters, the detailed clustering coefficient (Cp), normalized Cp (Gamma), characteristic path length (Lp), normalized Lp (Lambda), and small-world coefficient (Sigma) were determined. Meanwhile, the regional topological metrics, including nodal efficiency (Ne) and degree centrality (DC), were also obtained.

Statistical analysis

All statistical analyses were performed with custom-developed scripts in MATLAB (R2021b, MathWorks, USA).

For demographic and clinical data, analysis of variance (ANOVA) was applied for testing the group differences in age, education year, HIS, and clinical cognitive scores, and chi-squared test was employed to assess the group differences in sex, hypertension, diabetes, and lacunar infraction among HCs, SCD, and MCI groups.

To test the differences of each integrated network topological features among the 3 groups, analysis of covariate (ANCOVA) was first performed, with age as a covariate, and the *post-hoc* t-test was further conducted if a group difference was revealed. Moreover, Benjamini-Hochberg false discovery rate (FDR) correction was used to adjust for multiple comparisons to maintain an FDR <0.05.

Exploratory partial correlation analysis was applied to evaluate the associations of topological features, which exhibited significant differences among the 3 groups, with multiple clinical scales, using age as a covariate. Moreover, for network metrics presenting significant correlations with clinical scales, multiple stepwise regression analyses were subsequently used to further identify the significant topological predictors of cognitive performance, with age as a covariate. A P value <0.05 was considered to indicate statistical significance.

Results

Demographic and clinical characteristics

A total of 24 patients (13 SCD, 11 MCI) were excluded from the study. The final sample consisted of 25 (10 males

Table 1 Demographic and clinical characteristics of the participants

Variables	Group			P value (FDR corrected)
	HC (n=26)	SCD (n=25)	MCI (n=29)	
Age (years)	72.53±6.09	66.00±7.09	70.34±7.79	<0.01
Sex (M/F)	13/13	10/15	13/16	0.77
Education (years)	13.19±2.51	12.36±2.69	11.83±2.82	0.17
Hypertension (Y/N)	13/13	10/15	9/20	0.58
Diabetes (Y/N)	4/22	2/23	4/25	0.65
Lacunar infarction (Y/N)	0/26	0/25	0/29	1.00
HIS	1.19±0.49	1.40±0.76	1.34±0.72	0.52
MMSE	28.46±1.56[†]	27.48±1.56	26.72±11.58[§]	<0.01
TMT-A	60.73±19.41	67.96±17.76[‡]	90.34±28.37[§]	<0.01
TMT-B	154.42±49.37	153.12±43.46[‡]	228.93±65.04[§]	<0.01
BNT	23.88±2.92	23.24±3.24[‡]	18.21±4.95[§]	<0.01
AVFT	20.58±3.92[†]	17.72±3.84	15.76±5.77[§]	<0.01
AVLT-H (delayed recall)	4.31±1.87	4.84±2.37[‡]	1.97±2.24[§]	<0.01
AVLT-H (recognition)	21.77±1.75	21.24±2.00[‡]	18.31±2.54[§]	<0.01

Demographic and clinical data are demonstrated as mean ± standard deviation. Statistically significant differences: [†], between HC and SCD participants; [‡], between SCD and MCI participants; [§], between MCI and HC participants. FDR, false discovery rate; HC, healthy control; SCD, subjective cognitive decline; MCI, mild cognitive impairment; M, male; F, female; Y, yes; N, no; HIS, Hachinski Ischemic Scale; MMSE, Mini-mental State Examination; TMT-A, Trail Making Test part A; TMT-B, Trail Making Test part B; BNT, Boston Naming Test; AVFT, Animal Verbal Fluency Test; AVLT-H, Auditory Verbal Learning Test-Huashan version.

and 15 females) SCD patients and 29 (13 males and 16 females) MCI patients.

The demographic and clinical characteristics of the participants are listed in *Table 1*. There was no significant difference in sex, educational years, hypertension, diabetes, lacunar infraction, and HIS among the 3 groups, except for age (P<0.01). Statistically significant differences were observed in clinical cognitive performances among the 3 groups (P<0.01), including MMSE, delayed recall and recognition in Auditory Verbal Learning Test-Huashan version (AVLT-H), TMT A&B, AVFT, and BNT (FDR correction to maintain false positive error rate <0.05).

Comparison analysis of global topological features

Investigation of global topological feature variations was conducted via ANCOVA, using age as a covariate. Significant differences were revealed among the 3 groups in the metrics of Eg, Lp, and Lambda (all P<0.01). With further *post-hoc t*-test, a significant sequential decrease (all P<0.01) was seen in the Eg among the 3 groups. Meanwhile, there was a significant successive increase in the global metrics of Lp (all P<0.01) and Lambda (all P<0.05) among the 3 groups (FDR correction to maintain false positive error rate <0.05; *Table 2, Figure 1*). However, no statistically significant difference was observed in the global features of Eloc, Cp, Gamma, and Sigma among the 3 groups.

Comparison analysis of regional topological features

ANCOVA, with age as a covariate, was used to identify the group variations of regional topological features. Significant differences were shown in DC at the caudate nucleus (all P<0.01), Ne at the caudate nucleus, right insula, lenticular nucleus, and putamen (all P<0.05) among 3 groups. *Post-hoc t*-tests further revealed that, for the regional metric of DC, there was a significant successive decrease (all P<0.01) at the caudate nucleus and a sequential decrease (all P<0.01) in Ne at the left caudate nucleus. Furthermore, compared

Table 2 Statistically significant global topological features in all participants

Variables	Group			F	P value
	HC	SCD	MCI		
Eg	0.117±0.003	0.115±0.002	0.113±0.003	$F_{(2,77)}$ =17.95	<0.01
Lp	0.465±0.011	0.474±0.007	0.483±0.014	$F_{(2,77)}$ =17.97	<0.01
Lambda	0.264±0.005	0.268±0.004	0.272±0.006	$F_{(2,77)}$ =13.79	<0.01

Data are presented as mean ± standard deviation. HC, healthy control; SCD, subjective cognitive decline; MCI, mild cognitive impairment. Eg, global efficiency; Lp, characteristics path length; Lambda, normalized characteristics path length.
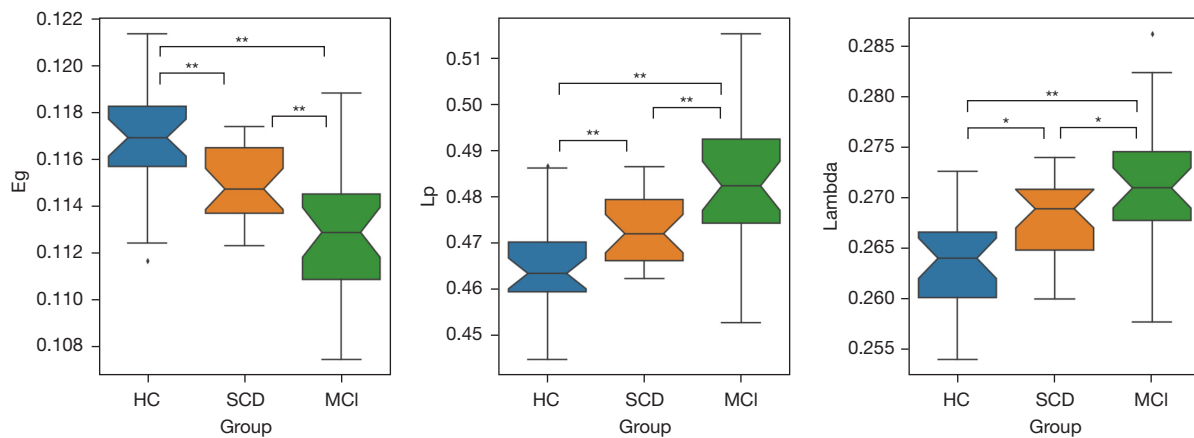
Figure 1 Box and whisker plots showing a significant sequential decrease in the global metric of Eg, and a significant increase in Lp and Lambda among three groups. Median (line within the box), the 25th and 75th percentiles (outer limits of each box) and the 5th and 95th percentiles (whiskers) are illustrated, with outliers plotted as dots. *, P<0.05; **, P<0.01. Eg, global metric of global efficiency; Lp, characteristics path length; Lambda, normalized characteristics path length; HC, healthy control; SCD, subjective cognitive to decline; MCI, mild cognitive impairment.

with HCs, SCD and MCI patients exhibited a significant decrease (all P<0.05) in Ne at the right insula. Compared with MCI participants, HCs and SCD cases showed a significant increase (all P<0.05) in Ne at regions of the right caudate nucleus, and lenticular nucleus, putamen, respectively (FDR correction to maintain false positive error rate <0.05; *Table 3, Figure 2*).

Association analysis of topological disturbances with clinical cognitive scales

The significant partial correlations between network metric alterations and clinical scales, when the age of participants was taken into account as a covariate, are displayed in *Table 4*. The partial correlation results showed that regional measurements of DC and Ne in caudate nucleus were statistically correlated with all clinical scales.

To further identify the significant topological predictors of cognitive performance, network metrics significantly correlated with clinical scales, including global and regional topology measurements, were subsequently used for multiple stepwise regression analysis. The stepwise regression model (*Table 5*) indicated that regional measurements of DC and Ne at caudate nucleus could statistically predict the cognition performance of HCs, SCD, and MCI patients (all P<0.05). However, no global topological metrics could significantly predict the cognitive performances.

Discussion

In the present study, the topological differences of normalized individual brain morphological networks, extracted in gray matter, were investigated among HCs and patients with SCD and MCI. Compared to HCs, both

Table 3 Statistically significant regional topological features in all participants

Variables and brain regions	Group			F	P value
	HC	SCD	MCI		
DC					
Left caudate nucleus	4.329±1.808	2.673±0.765	1.629±0.679	$F_{(2,77)}$ =35.72	<0.01
Right caudate nucleus	4.261±2.049	3.126±1.380	1.615±0.941	$F_{(2,77)}$ =21.31	<0.01
Ne					
Right insula	0.097±0.011	0.090±0.012	0.085±0.013	$F_{(2,77)}$ =6.64	0.04
Left caudate nucleus	0.119±0.017	0.103±0.013	0.074±0.024	$F_{(2,77)}$ =40.03	<0.01
Right caudate nucleus	0.119±0.020	0.106±0.018	0.070±0.028	$F_{(2,77)}$ =32.80	<0.01
Left lenticular nucleus, putamen	0.070±0.028	0.059±0.021	0.044±0.026	$F_{(2,77)}$ =7.24	0.03
Right lenticular nucleus, putamen	0.073±0.031	0.061±0.023	0.043±0.026	$F_{(2,77)}$ =8.68	0.01

Data are presented as mean ± standard deviation. HC, healthy control; SCD, subjective cognitive decline; MCI, mild cognitive impairment; DC, degree centrality; Ne, nodal efficiency.

SCD and MCI patients had altered network topology, which was characterized by significantly decreased Eg and longer Lp at the global level, and decreased DC and Ne at the regional level. The regional alterations were identified at caudate nucleus for DC, and at stratums and right insula for Ne. All these topological alterations were significantly associated with clinical cognitive scales, indicating that gray matter morphological networks could help to discriminate SCD and MCI patients from HCs. Overall, the individual morphological network abnormalities identified in this study highlighted clinically relevant alterations in the brain network topology for SCD and MCI patients. This may further provide evidence for the hypothesis that disruptions in brain connectivity result from synaptic dysfunction underlie cognitive decline.

Our findings of sequentially decreased Eg and increased Lp among the 3 groups of HC, SCD, and MCI indicated a successively decreased information integration in the brain morphological networks. The integration in network qualifies the ability to rapidly integrate specialized information from distributed brain regions (44), and the findings provide further evidence of the underlying mechanisms of disconnection in the AD spectrum. This damage of network topology was in line with the severity of cognitive impairment, illustrating that the Eg and Lp might serve as sensitive biomarkers in diagnosis of preclinical stages of AD. Our findings of abnormal global topology of the gray matter network in SCD and MCI were partly consistent with previous studies. Xue *et al.* [2020] found a

significant reduction in the amnestic MCI (aMCI) group on small-worldness and Eg based on the resting state fMRI (45), and Berlot *et al.* [2016] also showed that Eg and the mean Cp of networks were reduced in MCI by means of diffusion tensor imaging (DTI) (46). However, they found no significant difference in network topological properties between SCD patients and HCs. In our study, we revealed the damage of network topology in the SCD group, suggesting an earlier detection of disruption in preclinical stages of AD. With this finding, we may add new value to the previous understandings of a reduction in Eg of network structure in AD and MCI (47,48).

On the regional level, compared with HCs, decreased DC was identified at the caudate nucleus, and lower Ne was distributed at the caudate nucleus, right insula, and lenticular nucleus, putamen for SCD and MCI patients, respectively. This demonstrated a decreased regional centrality at these brain regions at preclinical stages of AD. The regional centrality metrics measure the importance of brain regions in interacting with other regions, facilitating information integration, and network resilience to insult (44,49). Yan *et al.* [2018] (50) found extensive disrupted rich club organization in MCI and AD patients based on DTI analysis. However, in SCD, aberrant connections were only found at the left caudate nucleus, middle frontal gyrus, orbital part, and the right caudate nucleus compared to HCs (50). The present study also found significantly different regional topological features at caudate nucleus, which was highly correlated with cognitive domains including executive,
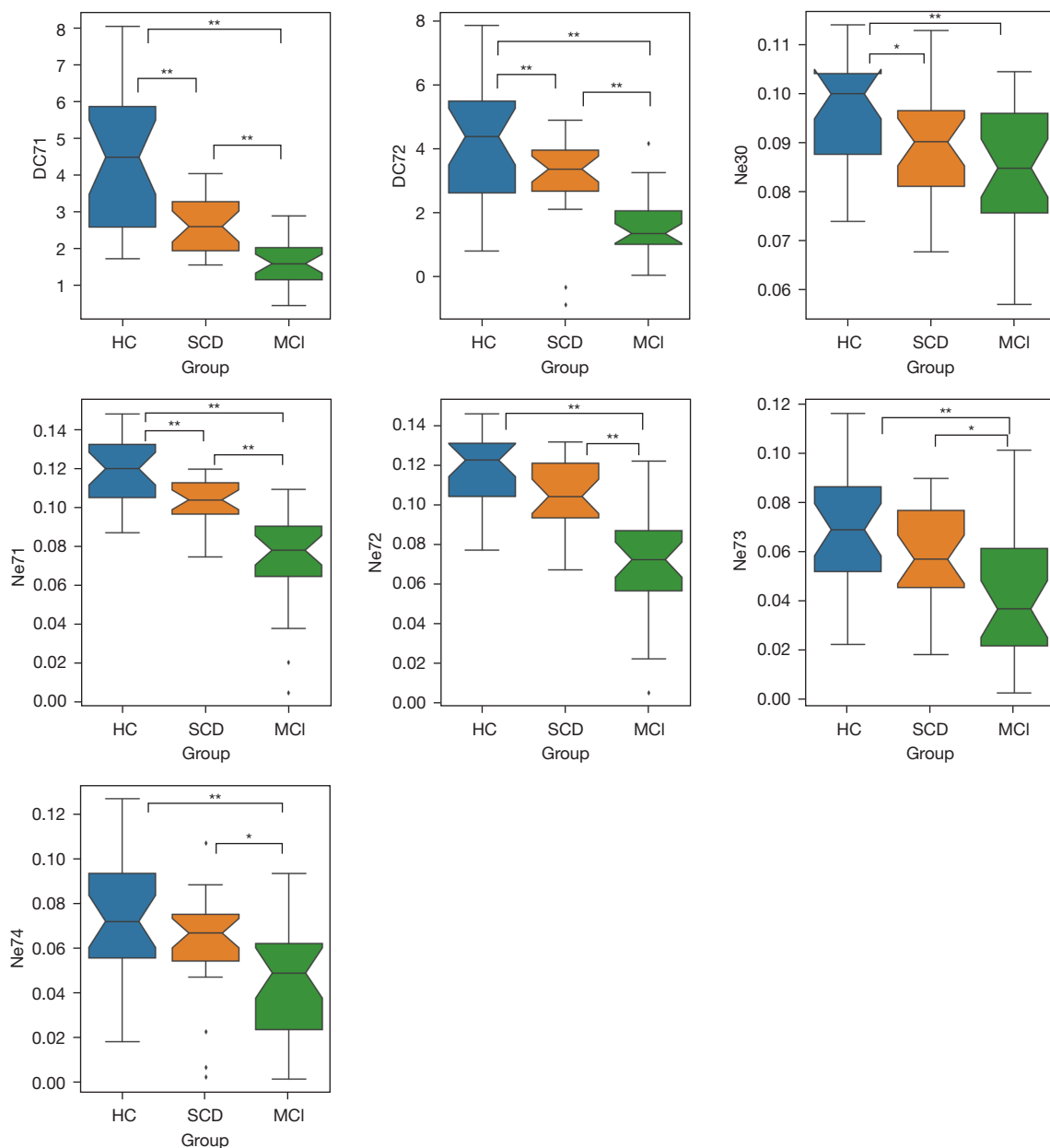
Figure 2 Box and whisker plots showing a significant sequential decrease in the nodal metrics of DC at the caudate nucleus [71, 72], and Ne at the left caudate nucleus [71]. Compared with HCs, participants with SCD and MCI exhibited significant decreases in Ne at the brain regions of right insula [30], right caudate nucleus [72], and lenticular nucleus, putamen, respectively [73, 74]. Median (line within the box), the 25th and 75th percentiles (outer limits of each box) and the 5th and 95th percentiles (whiskers) are illustrated, with outliers plotted as dots. *, P<0.05; **, P<0.01. 30, right insula; 71, left caudate nucleus; 72, right caudate nucleus; 73, right insula; 74, right lenticular nucleus, putamen. DC, degree centrality; Ne, nodal efficiency; HC, healthy control; SCD, subjective cognitive decline; MCI, mild cognitive impairment.

Table 4 Significant partial correlation between the altered topological properties and cognitive scales

Variables	TMT-B		AVFT		AVFT-H (delayed recall)	
	rho	P value	rho	P value	rho	P value
DC71	−0.39	<0.01	0.31	<0.01	0.32	<0.01
DC72	−0.33	<0.01	0.32	<0.01	0.29	<0.01
Ne30	–	–	0.28	0.013	–	–
Ne72	−0.45	<0.01	0.37	<0.01	0.34	<0.01
Ne73	−0.44	<0.01	0.42	<0.01	0.34	<0.01
Ne74	−0.22	0.047	0.25	0.029	–	–
Eg	–	–	0.34	<0.01	–	–
Lp	−0.39	<0.01	0.31	<0.01	–	–
Lambda	0.38	<0.01	−0.29	<0.01	–	–

30, right insula; 71, left caudate nucleus; 72, right caudate nucleus; 73, right insula; 74, right lenticular nucleus, putamen. TMT-B, Trail Making Test part B; AVFT, Animal Verbal Fluency Test; AVLT-H, Auditory Verbal Learning Test-Huashan version; DC, degree centrality; Ne, nodal efficiency; Eg, global efficiency; Lp, characteristics path length; Lambda, normalized characteristics path length.

Table 5 Stepwise regression analysis for clinical performance

Clinical performance and topological metric	Beta	P value	Adjusted R^2
TMT-B		<0.01	0.14
Ne71	−934.40	<0.01	
AVFT		<0.01	0.19
Ne30	81.50	0.049	
Ne72	61.11	<0.01	
AVLT-H (delayed recall)		<0.01	0.09
DC71	0.48	<0.01	

30, right insula; 71, left caudate nucleus; 72, right caudate nucleus. TMT-B, Trail Making Test part B; Ne, nodal efficiency; AVFT, Animal Verbal Fluency Test; AVLT-H, Auditory Verbal Learning Test-Huashan version; DC, degree centrality.

language, and memory in all participants. This finding aligned with those of previous studies that had shown that the caudate nucleus plays an important role in learning and working memory due to its heavy connection to the dorsolateral prefrontal cortex (51,52). It is also involved both in the integration of many sources of information along with instructions, and in the coordination of the transmission of information among cortical regions when no established pathways exist (53).

Previous studies have reported the right insula as a rich club which is the absolute network center, responsible for information exchange and integration (50). Our study also found the disturbance of right insula in SCD and MCI compared to HCs, indicating that the decreased Ne might reveal the pathology of the early AD spectrum.

The lenticular nucleus and putamen comprise the remaining parts of the striatum beside the caudate nucleus. The putamen has been found to be highly correlated with motor control (54). We found a weak correlation of the reginal topological parameters of the lenticular nucleus and putamen with executive and language domains. However, with age as a covariant, the correlation not significant according to multiple stepwise regression. This may be because the putamen does not dominate the executive

and language function but may assist in trial marking or language production during motor control of vocal organs.

Interestingly, the regional topological properties of DC and Ne outperformed the global topological metrics in predicting the cognition levels for HCs, SCD, and MCI. An explanation for this result might be that at the predementia stages of SCD and MCI, the morphological network alterations at specific brain regions are more significant compared with global topology alterations. With the clinical progression, the disturbance of global topological measurements may become more significant and severe.

In the present study, we applied a methodology recently proposed by Yu *et al.* [2018] (42) which normalizes the individual large-scale networks to a common framework, so that each individual network has the same network size. It has been confirmed that the size of network may have an effect on other network topological properties, and therefore, the normalization of individual networks may offer distinct advantages for comparative analyses (55). However, Tijms *et al.* [2014] (1) argued that the enforcement of identical network degree and size might introduce bias. Therefore, at this point, the question of how to fairly compare individual graphs with different size may remain open. The robustness of the 2 methods might be tested by further investigation using sophisticated machine learning classification algorithms on a large clinical cohort.

This study had some limitations. First, the sample size in our study was modest, and further verification of our findings should be conducted via a large clinical cohort. Second, the research was based on cross-sectional MRI data. A corresponding longitudinal study will be implemented to further monitor the alterations of individual morphological networks during the clinical progression. Third, although the construction of normalized individual morphological networks was based on the similarity of gray matter, the underlying physiological correlations of these structural network alterations remain unknown and need to be investigated in the future.

Conclusions

With the graphical analysis, this study demonstrated an altered topology in the normalized individual brain morphological network of SCD and MCI patients, compared with HCs. Their cognitive dysfunction was significantly related with the altered topological properties. Particularly, the regional centrality measurements of DC and Ne outperformed the global topological metrics

in predicting clinical cognitive performances for all participants. Therefore, these regional topological metrics might serve as biomarkers, to assist in identifying incipient brain damage at preclinical stages, namely, SCD and MCI, of AD.

Footnote

Conflicts of Interest: All authors have completed the ICMJE uniform disclosure form (available at https://qims.amegroups.com/article/view/10.21037/qims-22-1373/coif). WD and LQ are employees of GE Healthcare. The other authors have no conflicts of interest to declare.

Ethical Statement: The authors are accountable for all aspects of the work in ensuring that questions related to the accuracy or integrity of any part of the work are appropriately investigated and resolved. This study was conducted in accordance with the Declaration of Helsinki (as revised in 2013). The study was approved by Ethics Committee of the First Affiliated Hospital of Nanjing Medical University and written informed consent was provided by each of the participants.

Open Access Statement: This is an Open Access article distributed in accordance with the Creative Commons Attribution-NonCommercial-NoDerivs 4.0 International License (CC BY-NC-ND 4.0), which permits the non-commercial replication and distribution of the article with the strict proviso that no changes or edits are made and the original work is properly cited (including links to both the formal publication through the relevant DOI and the license). See: https://creativecommons.org/licenses/by-nc-nd/4.0/.

References

1. Tijms BM, Yeung HM, Sikkes SA, Möller C, Smits LL, Stam CJ, Scheltens P, van der Flier WM, Barkhof F. Single-subject gray matter graph properties and their relationship with cognitive impairment in early- and late-

5268

Ding et al. Identifying the preclinical stages of AD

onset Alzheimer's disease. Brain Connect 2014;4:337-46.

2. Cummings JL, Morstorf T, Zhong K. Alzheimer's disease drug-development pipeline: few candidates, frequent failures. Alzheimers Res Ther 2014;6:37.

3. Sanabria-Diaz G, Demonet JF, Rodriguez-Herreros B, Draganski B, Kherif F, Melie-Garcia L. Apolipoprotein E allele 4 effects on Single-Subject Gray Matter Networks in Mild Cognitive Impairment. Neuroimage Clin 2021;32:102799.

4. Jessen F, Amariglio RE, van Boxtel M, Breteler M, Ceccaldi M, Chételat G, et al. A conceptual framework for research on subjective cognitive decline in preclinical Alzheimer's disease. Alzheimers Dement 2014;10:844-52.

5. Rabin LA, Smart CM, Amariglio RE. Subjective Cognitive Decline in Preclinical Alzheimer's Disease. Annu Rev Clin Psychol 2017;13:369-96.

6. Jessen F, Amariglio RE, Buckley RF, van der Flier WM, Han Y, Molinuevo JL, Rabin L, Rentz DM, Rodriguez-Gomez O, Saykin AJ, Sikkes SAM, Smart CM, Wolfsgruber S, Wagner M. The characterisation of subjective cognitive decline. Lancet Neurol 2020;19:271-8.

7. Wang X, Huang W, Su L, Xing Y, Jessen F, Sun Y, Shu N, Han Y. Neuroimaging advances regarding subjective cognitive decline in preclinical Alzheimer's disease. Mol Neurodegener 2020;15:55.

8. Albert MS, DeKosky ST, Dickson D, Dubois B, Feldman HH, Fox NC, Gamst A, Holtzman DM, Jagust WJ, Petersen RC, Snyder PJ, Carrillo MC, Thies B, Phelps CH. The diagnosis of mild cognitive impairment due to Alzheimer's disease: recommendations from the National Institute on Aging-Alzheimer's Association workgroups on diagnostic guidelines for Alzheimer's disease. Alzheimers Dement 2011;7:270-9.

9. Jack CR Jr, Bennett DA, Blennow K, Carrillo MC, Dunn B, Haeberlein SB, et al. NIA-AA Research Framework: Toward a biological definition of Alzheimer's disease. Alzheimers Dement 2018;14:535-62.

10. Petersen RC. Mild cognitive impairment as a diagnostic entity. J Intern Med 2004;256:183-94.

11. Petersen RC. Mild cognitive impairment: transition between aging and Alzheimer's disease. Neurologia 2000;15:93-101.

12. Livingston G, Sommerlad A, Orgeta V, Costafreda SG, Huntley J, Ames D, et al. Dementia prevention, intervention, and care. Lancet 2017;390:2673-734.

13. Sperling RA, Aisen PS, Beckett LA, Bennett DA, Craft S, Fagan AM, et al. Toward defining the preclinical stages of Alzheimer's disease: recommendations from the National Institute on Aging-Alzheimer's Association workgroups on diagnostic guidelines for Alzheimer's disease. Alzheimers Dement 2011;7:280-92.

14. Toledo JB, Zetterberg H, van Harten AC, Glodzik L, Martinez-Lage P, Bocchio-Chiavetto L, et al. Alzheimer's disease cerebrospinal fluid biomarker in cognitively normal subjects. Brain 2015;138:2701-15.

15. van Harten AC, Smits LL, Teunissen CE, Visser PJ, Koene T, Blankenstein MA, Scheltens P, van der Flier WM. Preclinical AD predicts decline in memory and executive functions in subjective complaints. Neurology 2013;81:1409-16.

16. Jack CR Jr, Knopman DS, Jagust WJ, Petersen RC, Weiner MW, Aisen PS, Shaw LM, Vemuri P, Wiste HJ, Weigand SD, Lesnick TG, Pankratz VS, Donohue MC, Trojanowski JQ. Tracking pathophysiological processes in Alzheimer's disease: an updated hypothetical model of dynamic biomarkers. Lancet Neurol 2013;12:207-16.

17. Selkoe DJ. Alzheimer's disease is a synaptic failure. Science 2002;298:789-91.

18. Pereira JB, Mijalkov M, Kakaei E, Mecocci P, Vellas B, Tsolaki M, Kloszewska I, Soininen H, Spenger C, Lovestone S, Simmons A, Wahlund LO, Volpe G, Westman E. Disrupted Network Topology in Patients with Stable and Progressive Mild Cognitive Impairment and Alzheimer's Disease. Cereb Cortex 2016;26:3476-93.

19. Tijms BM, Kate MT, Wink AM, Visser PJ, Ecay M, Clerigue M, Estanga A, Garcia Sebastian M, Izagirre A, Villanua J, Martinez Lage P, van der Flier WM, Scheltens P, Sanz Arigita E, Barkhof F. Gray matter network disruptions and amyloid beta in cognitively normal adults. Neurobiol Aging 2016;37:154-60.

20. Yao Z, Zhang Y, Lin L, Zhou Y, Xu C, Jiang T; . Abnormal cortical networks in mild cognitive impairment and Alzheimer's disease. PLoS Comput Biol 2010;6:e1001006.

21. Tijms BM, Ten Kate M, Gouw AA, Borta A, Verfaillie S, Teunissen CE, Scheltens P, Barkhof F, van der Flier WM. Gray matter networks and clinical progression in subjects with predementia Alzheimer's disease. Neurobiol Aging 2018;61:75-81.

22. Alexander-Bloch AF, Gogtay N, Meunier D, Birn R, Clasen L, Lalonde F, Lenroot R, Giedd J, Bullmore ET. Disrupted modularity and local connectivity of brain functional networks in childhood-onset schizophrenia. Front Syst Neurosci 2010;4:147.

23. Liu Y, Liang M, Zhou Y, He Y, Hao Y, Song M, Yu C, Liu H, Liu Z, Jiang T. Disrupted small-world networks in

schizophrenia. Brain 2008;131:945-61.

24. Lo CY, Wang PN, Chou KH, Wang J, He Y, Lin CP. Diffusion tensor tractography reveals abnormal topological organization in structural cortical networks in Alzheimer's disease. J Neurosci 2010;30:16876-85.

25. Shu N, Liu Y, Li J, Li Y, Yu C, Jiang T. Altered anatomical network in early blindness revealed by diffusion tensor tractography. PLoS One 2009;4:e7228.

26. Li Y, Wang Y, Wu G, Shi F, Zhou L, Lin W, Shen D; . Discriminant analysis of longitudinal cortical thickness changes in Alzheimer's disease using dynamic and network features. Neurobiol Aging 2012;33:427.e15-30.

27. He Y, Chen Z, Evans A. Structural insights into aberrant topological patterns of large-scale cortical networks in Alzheimer's disease. J Neurosci 2008;28:4756-66.

28. Fu Z, Zhao M, He Y, Wang X, Lu J, Li S, Li X, Kang G, Han Y, Li S. Divergent Connectivity Changes in Gray Matter Structural Covariance Networks in Subjective Cognitive Decline, Amnestic Mild Cognitive Impairment, and Alzheimer's Disease. Front Aging Neurosci 2021;13:686598.

29. Tijms BM, Möller C, Vrenken H, Wink AM, de Haan W, van der Flier WM, Stam CJ, Scheltens P, Barkhof F. Single-subject grey matter graphs in Alzheimer's disease. PLoS One 2013;8:e58921.

30. Tijms BM, Yeung HM, Sikkes SA, Möller C, Smits LL, Stam CJ, Scheltens P, van der Flier WM, Barkhof F. Single-subject gray matter graph properties and their relationship with cognitive impairment in early- and late-onset Alzheimer's disease. Brain Connect 2014;4:337-46.

31. Tijms BM, Seriès P, Willshaw DJ, Lawrie SM. Similarity-based extraction of individual networks from gray matter MRI scans. Cereb Cortex 2012;22:1530-41.

32. Tijms BM, Sprooten E, Job D, Johnstone EC, Owens DG, Willshaw D, Seriès P, Lawrie SM. Grey matter networks in people at increased familial risk for schizophrenia. Schizophr Res 2015;168:1-8.

33. Niu R, Lei D, Chen F, Chen Y, Suo X, Li L, Lui S, Huang X, Sweeney JA, Gong Q. Disrupted grey matter network morphology in pediatric posttraumatic stress disorder. Neuroimage Clin 2018;18:943-51.

34. Batalle D, Muñoz-Moreno E, Figueras F, Bargallo N, Eixarch E, Gratacos E. Normalization of similarity-based individual brain networks from gray matter MRI and its association with neurodevelopment in infants with intrauterine growth restriction. Neuroimage 2013;83:901-11.

35. Dicks E, van der Flier WM, Scheltens P, Barkhof F,

Tijms BM; . Single-subject gray matter networks predict future cortical atrophy in preclinical Alzheimer's disease. Neurobiol Aging 2020;94:71-80.

36. Dicks E, Tijms BM, Ten Kate M, Gouw AA, Benedictus MR, Teunissen CE, Barkhof F, Scheltens P, van der Flier WM. Gray matter network measures are associated with cognitive decline in mild cognitive impairment. Neurobiol Aging 2018;61:198-206.

37. Folstein MF, Folstein SE, McHugh PR. "Mini-mental state". A practical method for grading the cognitive state of patients for the clinician. J Psychiatr Res 1975;12:189-98.

38. Zhao Q, Lv Y, Zhou Y, Hong Z, Guo Q. Short-term delayed recall of auditory verbal learning test is equivalent to long-term delayed recall for identifying amnestic mild cognitive impairment. PLoS One 2012;7:e51157.

39. Wang RY, Zhou JH, Huang YC, Yang YR. Reliability of the Chinese version of the Trail Making Test and Stroop Color and Word Test among older adults. International Journal of Gerontology 2018;12:336-9.

40. Ardila A. A cross-linguistic comparison of category verbal fluency test (ANIMALS): a systematic review. Arch Clin Neuropsychol 2020;35:213-25.

41. Chen TB, Lin CY, Lin KN, Yeh YC, Chen WT, Wang KS, Wang PN. Culture qualitatively but not quantitatively influences performance in the Boston naming test in a chinese-speaking population. Dement Geriatr Cogn Dis Extra 2014;4:86-94.

42. Yu K, Wang X, Li Q, Zhang X, Li X, Li S. Individual Morphological Brain Network Construction Based on Multivariate Euclidean Distances Between Brain Regions. Front Hum Neurosci 2018;12:204.

43. Wang J, Wang X, Xia M, Liao X, Evans A, He Y. GRETNA: a graph theoretical network analysis toolbox for imaging connectomics. Front Hum Neurosci 2015;9:386.

44. Rubinov M, Sporns O. Complex network measures of brain connectivity: uses and interpretations. Neuroimage 2010;52:1059-69.

45. Xue C, Sun H, Hu G, Qi W, Yue Y, Rao J, Yang W, Xiao C, Chen J. Disrupted Patterns of Rich-Club and Diverse-Club Organizations in Subjective Cognitive Decline and Amnestic Mild Cognitive Impairment. Front Neurosci 2020;14:575652.

46. Berlot R, Metzler-Baddeley C, Ikram MA, Jones DK, O'Sullivan MJ. Global Efficiency of Structural Networks Mediates Cognitive Control in Mild Cognitive Impairment. Front Aging Neurosci 2016;8:292.

47. Reijmer YD, Leemans A, Caeyenberghs K, Heringa SM, Koek HL, Biessels GJ; . Disruption of cerebral networks and cognitive impairment in Alzheimer disease. Neurology 2013;80:1370-7.

48. Bai F, Shu N, Yuan Y, Shi Y, Yu H, Wu D, Wang J, Xia M, He Y, Zhang Z. Topologically convergent and divergent structural connectivity patterns between patients with remitted geriatric depression and amnestic mild cognitive impairment. J Neurosci 2012;32:4307-18.

49. Ye M, Yang T, Qing P, Lei X, Qiu J, Liu G. Changes of Functional Brain Networks in Major Depressive Disorder: A Graph Theoretical Analysis of Resting-State fMRI. PLoS One 2015;10:e0133775.

50. Yan T, Wang W, Yang L, Chen K, Chen R, Han Y. Rich club disturbances of the human connectome from subjective cognitive decline to Alzheimer's disease. Theranostics 2018;8:3237-55.

51. Levitt JJ, McCarley RW, Dickey CC, Voglmaier MM, Niznikiewicz MA, Seidman LJ, Hirayasu Y, Ciszewski AA, Kikinis R, Jolesz FA, Shenton ME. MRI study of caudate nucleus volume and its cognitive correlates in neuroleptic-naive patients with schizotypal personality disorder. Am J Psychiatry 2002;159:1190-7.

52. Levy R, Friedman HR, Davachi L, Goldman-Rakic PS. Differential activation of the caudate nucleus in primates performing spatial and nonspatial working memory tasks. J Neurosci 1997;17:3870-82.

53. Stocco A, Lebiere C, O'Reilly RC, Anderson JR. Distinct contributions of the caudate nucleus, rostral prefrontal cortex, and parietal cortex to the execution of instructed tasks. Cogn Affect Behav Neurosci 2012;12:611-28.

54. Haber SN. Corticostriatal circuitry. Dialogues Clin Neurosci 2016;18:7-21.

55. van Wijk BC, Stam CJ, Daffertshofer A. Comparing brain networks of different size and connectivity density using graph theory. PLoS One 2010;5:e13701.